NASA TECHNICAL NOTE

NASA TN D-8223

NASA TN D-8223

CALCULATION OF WIND-DRIVEN SURFACE CURRENTS IN THE NORTH ATLANTIC OCEAN

Thomas H. Rees and Richard E. Turner

Langley Research Center
Hampton, Va. 23665

NATIONAL AERONAUTICS AND SPACE ADMINISTRATION • WASHINGTON, D. C. • JUNE 1976

1. Report No.	2. Government Accession No.	3. Recipient's Catalog No.
NASA TN D-8223		

4. Title and Subtitle	5. Report Date
CALCULATION OF WIND-DRIVEN SURFACE CURRENTS IN THE NORTH ATLANTIC OCEAN	June 1976
	6. Performing Organization Code
7. Author(s)	8. Performing Organization Report No.
Thomas H. Rees and Richard E. Turner	L-10740
	10. Work Unit No.
9. Performing Organization Name and Address	176-30-31-00
NASA Langley Research Center Hampton, Va. 23665	11. Contract or Grant No.
	13. Type of Report and Period Covered
12. Sponsoring Agency Name and Address	Technical Note
National Aeronautics and Space Administration Washington, D.C. 20546	14. Sponsoring Agency Code

15. Supplementary Notes

16. Abstract

Calculations to simulate the wind-driven near-surface currents of the North Atlantic Ocean are described. The primitive equations were integrated on a finite-difference grid with a horizontal resolution of 2.5° in longitude and latitude. The model ocean was homogeneous with a uniform depth of 100 m and with five levels in the vertical direction. A form of the rigid-lid approximation was applied. Generally, the computed surface current patterns agreed with observed currents. The development of a subsurface equatorial countercurrent was observed.

17. Key Words (Suggested by Author(s))	18. Distribution Statement
Numerical modeling Ocean dynamics North Atlantic Ocean Wind-driven currents	Unclassified – Unlimited Subject Category 48

19. Security Classif. (of this report)	20. Security Classif. (of this page)	21. No. of Pages	22. Price*
Unclassified	Unclassified	23	$3.25

*For sale by the National Technical Information Service, Springfield, Virginia 22161

CALCULATION OF WIND-DRIVEN SURFACE CURRENTS IN THE NORTH ATLANTIC OCEAN

Thomas H. Rees and Richard E. Turner
Langley Research Center

SUMMARY

Calculations to simulate the wind-driven near-surface currents of the North Atlantic Ocean during Northern Hemisphere summer are described. A computer simulation program, based upon a primitive equation formulation, was used to integrate the equations of motion on a finite-difference grid with 2.5^{o} resolution. The model ocean was homogeneous with a uniform depth of 100 m, with five levels in the vertical direction, and with a constrained upper surface. The equations were integrated for approximately 40 simulation days, at which time the computed surface currents agreed generally with observed currents. The development of a subsurface equatorial countercurrent at the 90-m level was observed.

INTRODUCTION

A number of problem areas exist today which involve the interaction between the environment and man's activities. Of particular concern are the injection and subsequent dispersal of manmade pollutants in the atmosphere and in the surface waters of the globe.

Consequently, an effort was begun at the Langley Research Center to develop a generalized circulation model suitable for simulation of both atmospheric and oceanic circulation on a wide range of scales. A generalized tensor formulation of the primitive equations (conservation of mass and momentum and transport of conservable scalars) was derived in reference 1. This formulation provides a set of transport equations common to the atmosphere and ocean by using similar coordinate systems and by assuming both to be in hydrostatic equilibrium in the vertical direction. Separate but similar computer models based upon the generalized formulation were written for the atmosphere and the ocean. A detailed discussion of the ocean dynamics model is presented in reference 2.

Because large-scale changes in the open ocean occur slowly, a common practice in ocean modeling to improve computational efficiency is to adopt a "rigid-lid" approximation in which the vertical velocity is set identically to zero at the sea surface. This effectively removes surface gravity waves, without appreciably affecting the steady circulation patterns, and thereby allows time increments to be orders of magnitude larger than would otherwise have been possible with simple explicit numerical schemes. However, the

application of a rigid lid has in the past generally led to formulation of the equations of motion in terms of a stream function. (See ref. 3, for example.) A consequence of the stream function approach is that a Poisson boundary value problem must be solved for the stream function around land-mass boundaries. Islands greatly complicate the solution.

The model of reference 2 combines a general formulation of the primitive equations with a new rigid-lid approximation. Land boundaries are handled much more simply than in a stream function model, while the advantage of a longer time step is retained.

The purpose of the present work is to provide preliminary validation of the ocean circulation model of reference 2. For the purpose of this report, preliminary validation consists of (1) demonstrating long-term stability of the computer model, (2) demonstrating convergence of the model to an equilibrium state, and (3) verifying that the results of the calculations agree with the observed data to an accuracy commensurate with the model spatial resolution.

The approach taken was to define an idealized model of a closed basin. The circulation of the North Atlantic Ocean was chosen for simulation because of the availability of observational data and because at least the surface layer could be isolated from other bodies of water without severely affecting the results. A grid spacing of 2.5° in longitude and latitude was chosen as a compromise between finer resolution and increased computer requirements. The ocean was idealized to be homogeneous in density, to be shallow and of uniform depth, and to be driven only by a summer mean wind stress distribution.

SYMBOLS

A	determinant of quasi-horizontal metric tensor
C_D	drag coefficient for bottom friction calculations
F_α	mixing, centrifugal, and incremental Coriolis force terms, defined by equations (4) and (5), N
f	Coriolis parameter
g_{jj}	covariant element of the metric tensor
K_H	horizontal subgrid mixing coefficient, m^2/sec
K_o	Von Kármán constant, 0.4
K_V	vertical subgrid mixing coefficient, m^2/sec

$\hat{\ell}^i{}_j$	mixed tensor components of deviatoric strain-rate tensor, defined by equation (8)
P	pressure, N/m^2
P_c	surface constraint pressure, N/m^2
P_f	approximate hydrostatic pressure referenced to mean sea level (flat top) geoid, N/m^2
r	mean radius of the Earth, m
S	salinity, parts per thousand $\left(^o/_{oo}\right)$
S_j	physical velocity of coordinate grid points relative to rotating Earth, m/sec
T	temperature, ^oC
t	time, sec
U_j	physical component of fluid velocity relative to rotating Earth, m/sec
U_j'	turbulent part of U_j, m/sec
$\tilde{U}_\alpha$	approximate value of U_α, m/sec
V_j	physical component of fluid velocity relative to coordinate frame of reference, m/sec
X^3	depth of ocean in transformed coordinates
x^j	coordinates of reference coordinate system (see fig. 1)
Δ	mixing length for subgrid diffusion
ζ	generalized density, $\rho\sqrt{g_{33}}$
ξ	specifies layer thickness distribution as a function of x^3
ρ	density of sea water, kg/m^3

ρ_o reference density, 10^3 kg/m^3

τ_α components of wind stress, N/m^2

ψ variable of integration

ω angular velocity of the Earth, rad/sec

Indices:

i,j take on values 1, 2, or 3

α takes on values 1 or 2 only

1,2,3 particular coordinate direction

Notation:

$<>$ space average over a grid cell and time average over a time step

$( )_{,j}$ partial derivative of ( ) with respect to x^j; for example, $P_{,2} = \frac{\partial P}{\partial x^2}$

MATHEMATICAL MODEL

The generalized circulation model described in reference 1 is a tensor formulation of the so-called primitive equations, the equations representing conservation of mass, momentum, salinity, and internal energy. The formulation makes use of the hydrostatic approximation, which neglects local acceleration in the equation of motion for vertical velocity; the momentum equation in the vertical direction is replaced by the hydrostatic and continuity equations. This approximation is quite common in large-scale circulation modeling because it allows a much longer integration time step. Some notable features of the mathematical formulation are

(1) Combining density and the vertical scale factor to form a generalized density

(2) Distortion of the quasi-horizontal bottom coordinate surface to follow the Earth's topography and provision for vertical motion of the other quasi-horizontal surfaces

(3) Projection of gravity onto the quasi-horizontal surfaces

(4) Derivation of an improved subgrid diffusion equation

(5) Use of generalized density rather than pressure or density as a dependent variable

The ocean circulation model described in detail in reference 2 is an extension of the generalized formulation of reference 1. The following two approximations, both of which are common in ocean modeling, are made:

(1) The Boussinesq approximation, which neglects density variations except in the buoyancy term and in the hydrostatic equation

(2) An empirical equation of state, giving density as a function of pressure, temperature, and salinity, is assumed.

The ocean model has the capability to operate as an unfiltered primitive equation model (as a free-surface model) or as a filtered model (with the rigid-lid approximation). Land boundaries and bottom topography are modeled simply.

In this report the dynamic equations are presented in somewhat simplified form. For example, since the present study makes use of the rigid-lid approximation, terms dealing with motion of the grid structure are omitted. Terms in the momentum equations arising from variation in depth have also been omitted. Since the present study deals with a homogeneous ocean, the transport equations and boundary conditions for salinity and internal energy are omitted. Equations have been combined when feasible. The reader interested in a rigorous derivation of the generalized model is referred to reference 1, and the reader interested in a more detailed description of the ocean model, including the rigid-lid approximation and the numerical technique employed, is referred to reference 2.

Coordinate System

The coordinate system (fig. 1) chosen for the ocean model is described in detail in reference 1. The lower coordinate surface $\left(x^3 = 0\right)$ follows the ocean floor, while the upper coordinate surface $\left(x^3 = X^3\right)$ follows the upper surface of the ocean. For the present case of a uniform-depth ocean with a constrained upper surface, the reference frame reduces to spherical polar coordinates. The coordinate x^1 represents colatitude and x^2 represents longitude. The gravity vector coincides with the local x^3 parametric line.

In appendix B of reference 1, it is shown that the differential geometry of the coordinate system is sufficiently represented by the approximate metric tensor

$$g_{11} = r^2$$

$$g_{22} = \left(r \sin x^1\right)^2$$

$$g_{33} = g_{33}\left(x^1, x^2, x^3, t\right)$$

where r is the Earth's radius, assumed constant everywhere. The determinant of the quasi-horizontal metric tensor is simply

$$A = g_{11}g_{22}$$

The conservation equations are formulated in terms of a generalized density $\zeta = \rho\sqrt{g_{33}}$, and applying the Boussinesq approximation $(\rho = \rho_o)$ results in

$$\zeta = \rho_o\sqrt{g_{33}}$$

where $\sqrt{g_{33}}$ is the vertical scale factor. The rigid-lid approximation described in reference 2 negates long-term depth variations, so that the time-averaged motion of the coordinate system relative to the rotating Earth is zero. However, although the horizontal components of grid velocity S_α are negligible, the instantaneous vertical grid velocity S_3 must be considered, so that

$$V_\alpha = U_\alpha$$

$$V_3 = U_3 - S_3$$

The spatial derivative $S_{3,\alpha}$ is ignored.

Dynamic Equations

If substitutions are made according to the foregoing approximations, then the continuity equation given in reference 1 as equation (1) may be written as

$$\frac{\partial\zeta}{\partial t} + \frac{1}{r \sin x^1}\left[\left(\zeta U_1 \sin x^1\right)_{,1} + \left(\zeta U_2\right)_{,2}\right] + \rho_o V_{3,3} = 0 \qquad (1)$$

The second and third terms on the left side of equation (1) represent horizontal and vertical divergence, respectively. Similarly, the dynamic equation for momentum conservation in the x^1-direction (south direction) given in reference 1 as equation (2) may be written as

$$\frac{\partial}{\partial t}\left(\zeta U_1\right) + \frac{1}{r \sin x^1}\left[\left(\zeta U_1 U_1 \sin x^1\right)_{,1} + \left(\zeta U_1 U_2\right)_{,2}\right] + \rho_o\left(U_1 V_3\right)_{,3}$$

$$= -\frac{\zeta}{\rho_o r} P_{,1} + \zeta f U_2 - F_1 \qquad (2)$$

where the Coriolis parameter f is given by

$$f = 2\omega \cos x^1$$

and where the subgrid diffusion and centrifugal force terms are grouped into F_1. The corresponding equation in the x^2 direction (east direction) given as equation (3) of reference 1 may be written as

$$\frac{\partial}{\partial t}\left(\zeta U_2\right) + \frac{1}{r \sin x^1}\left[\left(\zeta U_1 U_2 \sin x^1\right)_{,1} + \left(\zeta U_2 U_2\right)_{,2}\right] + \rho_o\left(U_2 V_3\right)_{,3} = -\frac{\zeta}{\rho_o r \sin x^1} P_{,2} - \zeta f U_1 - F_2 \tag{3}$$

The terms F_1 and F_2 from equations (2) and (3) may be written explicitly as

$$F_1 = \frac{1}{r \sin x^1}\left[\left(\zeta\left\langle U_1' U_1'\right\rangle \sin x^1\right)_{,1} + \left(\zeta\left\langle U_1' U_2'\right\rangle\right)_{,2}\right] + \rho_o\left(\left\langle U_1' U_3'\right\rangle\right)_{,3} - \left(U_2 U_2 + \left\langle U_2' U_2'\right\rangle\right)\frac{\zeta \cot x^1}{r} \tag{4}$$

$$F_2 = \frac{1}{r \sin x^1}\left[\left(\zeta\left\langle U_1' U_2'\right\rangle \sin x^1\right)_{,1} + \left(\zeta\left\langle U_2' U_2'\right\rangle\right)_{,2}\right] + \rho_o\left(\left\langle U_2' U_3'\right\rangle\right)_{,3} + \left(U_1 U_2 + \left\langle U_1' U_2'\right\rangle\right)\frac{\zeta \cot x^1}{r} \tag{5}$$

The terms on the right side of equations (4) and (5) represent horizontal and vertical subgrid mixing and the contribution of U_2 to centrifugal and Coriolis forces. The primed quantities indicate the turbulent parts (i.e., the difference between the instantaneous values and the space-time averages), and the brackets $\langle\ \rangle$ indicate space averaging over a nodal cell and time averaging over a time step. The horizontal subgrid mixing is parametrized by a nonlinear kinematic eddy viscosity theory, wherein the subgrid velocity correlations are, from equations (8) and (9) of reference 1,

$$\left.\begin{aligned}\left\langle U_1' U_1'\right\rangle &= -K_H \hat{\ell}^1{}_1 \\ \left\langle U_1' U_2'\right\rangle &= -\frac{K_H \hat{\ell}^1{}_2}{\sin x^1} \\ \left\langle U_2' U_2'\right\rangle &= -K_H \hat{\ell}^2{}_2\end{aligned}\right\} \tag{6}$$

The kinematic eddy viscosity K_H given in equation (11) of reference 1 may be expanded and rewritten as

$$K_H = 2(K_o\Delta)^2\left(\hat{\ell}^1{}_1\hat{\ell}^1{}_1 + \hat{\ell}^1{}_2\hat{\ell}^2{}_1\right)^{1/2} \tag{7}$$

where K_o is the Von Kármán constant for turbulent mixing, and Δ is a characteristic mixing length. The required components of the strain-rate tensor are, from equation (7) of reference 1,

$$\left.\begin{aligned}
\hat{\ell}^1{}_1 &= \frac{1}{r \sin x^1}\left[\left(U_1 \sin x^1\right)_{,1} - U_{2,2} - 2U_1 \cos x^1\right] \\
\hat{\ell}^1{}_2 &= \frac{1}{r}\left[\left(U_2 \sin x^1\right)_{,1} + U_{1,2} - 2U_2 \cos x^1\right] \\
\hat{\ell}^2{}_1 &= \frac{\hat{\ell}^1{}_2}{\left(\sin x^1\right)^2} \\
\hat{\ell}^2{}_2 &= -\hat{\ell}^1{}_1
\end{aligned}\right\} \tag{8}$$

The vertical subgrid mixing is parametrized by a much simpler technique, wherein a mixing coefficient is specified. By combination of equations (12), (13), and (7) of reference 1, the velocity correlations in the vertical mixing terms of equations (4) and (5) may be written as

$$\left.\begin{aligned}
\left\langle U_1' U_3' \right\rangle &= -\frac{\rho_o K_V}{\zeta} U_{1,3} \\
\left\langle U_2' U_3' \right\rangle &= -\frac{\rho_o K_V}{\zeta} U_{2,3}
\end{aligned}\right\} \tag{9}$$

where the mixing coefficient K_V may vary with depth. At the lower boundary, the conditions, from reference 2,

$$\left.\begin{aligned}
\left\langle U_1' U_3' \right\rangle &= -C_D U_1\left[\left(U_1\right)^2 + \left(U_2\right)^2\right]^{1/2} \\
\left\langle U_2' U_3' \right\rangle &= -C_D U_2\left[\left(U_1\right)^2 + \left(U_2\right)^2\right]^{1/2}
\end{aligned}\right\} \tag{10}$$

are applied to equations (9), while at the upper surface the wind stress

$$\tau_1 = \rho_o\left\langle U_1' U_3' \right\rangle \qquad\qquad \tau_2 = \rho_o\left\langle U_2' U_3' \right\rangle \tag{11}$$

is a driving boundary condition (forcing function).

The vertical velocity V_3 required in equations (1), (2), and (3) at a given location (x^1,x^2) may be computed as

$$V_3(x^3) = \frac{\xi(x^3)}{\rho_o r \sin x^1} \int_0^{X^3} \left[(\zeta U_1 \sin x^1)_{,1} + (\zeta U_2)_{,2} \right] dx^3$$

$$- \frac{1}{\rho_o r \sin x^1} \int_0^{x^3} \left[(\zeta U_1 \sin x^1)_{,1} + (\zeta U_2)_{,2} \right] d\psi$$

$$= -S_3(x^3) + U_3(x^3) \qquad (12)$$

where $\xi(x^3)$ is the ratio of the local height above the sea floor to the total ocean depth. Equation (12) follows from equation (15) of reference 1 with the boundary conditions,

$U_3 = V_3 = 0$ at the lower boundary $(x^3 = 0)$

$V_3 = 0$ at the upper boundary $(x^3 = X^3)$

and with the restriction of equally spaced layers, or more generally, with $S_3(x^3)$ proportional to the local height above the sea floor.

Land-Sea Boundaries

In the present work, the boundary condition applied at model land-sea boundaries is simply that the mass transport normal to such a boundary in a water column adjacent to the boundary is zero. This condition is automatically satisfied by requiring the depth to slope to zero at a nodal point instead of between nodal points, so that $\sqrt{g_{33}}$ and ζ vanish identically along the beachline. Thus, the coastline always follows a parametric line connecting two nodal points. The continental boundaries in this system are series of steps.

When the rigid-lid approximation is used, an additional boundary condition – that the mass transport normal to the beach in a water column adjacent to a land boundary is zero – is required. This condition is imposed by adjusting the horizontal velocity components throughout the column to yield a net transport of zero for the column.

Air-Sea Interface

For the present study, the wind stress on the upper surface was chosen as the driving condition. Other boundary conditions at the air-sea interface (evaporation, precipitation, and heat transport) were zero.

Surface Constraint Pressure

In reference 2, it is stated that the pressure is given by

$$P = P_f + P_c$$

where P_f is an approximate hydrostatic pressure referenced to the mean sea level geoid (i.e., the flat top depth) and P_c is the surface constraint pressure. In the empirical equation of state, $\rho = \rho(P,S,T)$, the compressibility effects of P_c are ignored. Thus, for the case of a homogeneous, uniform-depth basin as presented herein, $P_{f,\alpha} = 0$, or in equations (2) and (3), $P_{,\alpha} = P_{c,\alpha}$. The surface pressure P_c is computed iteratively as described in reference 2.

NUMERICAL SOLUTION

The mathematical model was programed for a digital computer in finite-difference notation and integrated on a three-dimensional grid. This integration technique used central differencing in time and space, with the horizontal grid structure split into two time layers.

Application of the rigid-lid constraint is achieved by dividing the integration into two distinct stages. The first stage computes approximate values of U_α over the entire lattice by setting $P_c = 0$. In the second stage, these approximate velocities are corrected to enforce zero local horizontal divergence. The sequence of computations is summarized as follows:

(1) V_3 is computed from equation (12).

(2) $\frac{\partial \zeta}{\partial t}$ is computed from equation (1).

(3) $\frac{\partial}{\partial t}(\zeta U_\alpha)$ are computed from equations (2) to (11) with $P_c = 0$ (no pressure gradient force).

(4) ζ is updated.

(5) U_α are updated to approximate values $\tilde{U}_\alpha$.

(6) Boundary conditions at lateral land-sea boundaries are applied.

(7) P_c is computed by relaxation to yield values of $\frac{\partial}{\partial t}(\zeta \tilde{U}_\alpha)$ which force the solution to zero local horizontal divergence.

(8) $\tilde{U}_\alpha$ are updated to the corrected values U_α.

The numerical technique is discussed in more detail in reference 2.

NORTH ATLANTIC BASIN MODEL

A lattice spacing that would give reasonably good definition of large-scale flow features was sought. A 2.5° by 2.5° grid spacing in longitude and latitude was adopted as a compromise between finer resolution and increased computer requirements. The decision to model the North Atlantic Ocean in isolation from other oceans required the use of either open boundaries or artificially closed boundaries at the north and south grid limits. The latter were chosen for simplicity. Also, a closed system was considered to have advantages for validation purposes.

The choice of artificial boundary locations was not arbitrary. Boundaries were sought at which the flow along the boundary would, in the real world, be predominately parallel to the artificial boundary and/or at which the mass transport across the boundary would be minimal. It was recognized that near 7° to 8° south latitude the surface current (the South Equatorial Current) is essentially zonal. (See fig. 2 which was reproduced from ref. 4 by permission of publisher.) This location was therefore deemed a reasonable choice for an artificial boundary in a surface-layer model. (Since the deep currents near the Equator are predominately meridional, the 7° to 8° latitudes would not have been a good choice for a closed boundary for a deep-ocean model.) For the northern boundary, 80° north latitude was considered a reasonable choice because the north-south surface transport is small there. The grid used for the present calculations is shown in figure 3. As indicated, the grid encloses the region from 82.5° north to 10° south and from 100° west to 20° east. The computational grid was composed of 48 points in the east-west direction and 37 points in the north-south direction.

MODEL PARAMETERS

The input parameters for the present study are summarized in table I. The lattice spacing of 2.5° in longitude and latitude is equivalent near the Equator to a square mesh with 278 km between grid points, whereas at 80° north the resolution in the east-west direction is approximately 48 km. (This resolution tends to smear the boundaries of strong currents such as the Gulf Stream.) The model had five layers for the present study with a uniform depth of 100 m. Each layer was 20 m thick.

For the present calculations, the wind stress field was interpolated from tables of the summer mean presented by Hellerman in reference 5. The applied wind stress vector field is shown in figure 4. The pattern of figure 4 represents the Northern Hemisphere summer mean wind stress based on wind-rose data given in U.S. Navy atlases. The wind stress data in reference 5 were tabulated on a 5° grid and extended only to 72.5° north. The data presented in figure 4 were interpolated onto the present grid system. Note, however, that the data were not extrapolated into the most northern latitudes, and that the

applied wind stress east and west of Greenland is very low. (These areas are largely covered with ice in the real world.)

Because of the high level of turbulence in the wind-driven surface layers, the vertical mixing coefficient for momentum transport K_V was taken as 0.01 m^2/sec. This value of K_V agrees with that used for the upper 100 m in reference 3. The Von Kármán constant K_o in equation (7) was taken as 0.4. The drag coefficient C_D in equation (10), normally taken as approximately 0.002, was taken herein as 10^{-4} in an attempt to simulate the lower resistance of the water at 100 m as opposed to the resistance of a real bottom.

The salinity and temperature fields were set to standard ocean conditions ($S = 35\ ^{o}/_{oo}$ and $T = 0^{o}\ C$) and held constant. The velocity field was initially zero. The kinetic energy in the entire field was monitored as a convergence check.

RESULTS

The dynamic equations of motion were integrated numerically on a digital computer starting from a state of rest. The initial response to the wind stress was development of a large, slow-moving clockwise gyre centered near the geographic center of the ocean. As simulation time progressed, this gyre strengthened, the gyre center moved westward, and the western boundary currents intensified.

Three horizontal velocity vector fields are presented in figure 5. This figure represents the computed, nearly steady-state currents after approximately 40 simulation days. The currents in the surface layer (0 to 20 m) are shown in figure 5(a); those in the bottom layer (80 to 100 m), in figure 5(b); and the vertically averaged horizontal currents, in figure 5(c). The time derivatives from the momentum equations were smoothed zonally to control numerical problems arising from convergence of the x^1 parametric lines near the pole. This smoothing was applied heavily at the most northern latitudes, but was not applied at all near the Equator.

Toward the end of the simulation, significant numerical problems arose in the region east of Greenland from about 60^{o} north to the northern limit of the model. Within 3 simulation days after the time period shown in figure 5, the velocities along the two most northern nodal lines began increasing exponentially. For approximately 12 days prior to this, however, the entire field was essentially in steady state. The high-latitude instability probably occurred because of the minimal applied wind stress in that region (fig. 4). The disorganized motion in the region was driven by diffusion, and thus no predominant pattern existed.

Two other aspects of the model, grid resolution and land boundary treatment, warrant attention. A second-order accurate finite-difference technique such as the one used herein tends to spread strong gradients over about five nodal points. Thus, strong currents (the

Gulf Stream, for example) are much wider in the computed current field than in the real world and have a lower maximum current speed. The land boundary treatment in the present model is to set the vertically integrated horizontal transport momentum normal to a boundary equal to zero by adjusting the horizontal velocity in each layer. Tests for land boundaries are carried out along x^1 and x^2 parametric lines, and the model sees irregular continental boundaries as series of steps. Consequently, strong boundary currents are affected in three ways. First, since the momentum adjacent to the boundary is reduced at a boundary step, the momentum of the current may be significantly reduced. Second, reducing the current velocity next to a land boundary increases the shoreward current gradient. As a result, on a finite-difference grid, the current is forced out from the boundary by approximately one nodal distance. And third, a step change in the lateral boundary, especially a double step, can cause a strong boundary current to be deflected 90°.

The prominent features of computed surface current patterns shown in figure 5(a) agree for the most part with the corresponding features of the observed data. (See fig. 2.) A rough quantitative comparison of the computed and observed current speeds for some of the major currents is presented in table II.

In figure 5(a), the westerly South Equatorial Current (1) in the most southern latitudes is well developed, even though in the model it must be fed principally by overturning. (The Benguela Current, which flows northward off the coast of South Africa to feed the South Equatorial Current in the observed data, is not modeled because the southern boundary is closed.) The South Equatorial Current splits near the east coast of South America, with part turning back to form the Equatorial Countercurrent (2) and part continuing up the coast. The weakness of the coastal current may have been due in part to the stepwise representation of the land geometry and land boundary treatment which combine to turn the flow northward. The observed South Equatorial Current (fig. 2) also splits, the southward branch forming the Brazil Current. The wind stress (fig. 4) along the three most southern latitudes of the model is directed toward the west-northwest. Since these latitudes (1.25° to 6.25° south) are in the Southern Hemisphere, Coriolis acceleration acts to the left; the result along the closed boundary is a current with a small southerly component. The flow is blocked by the artificial southern boundary, however, and merely sinks. The North Equatorial Current (3) splits also, with part flowing south of Cuba and the rest to the north of Cuba. The two segments rejoin in the Florida Current. The Gulf Stream (4) and the North Atlantic Current (5) are also easily recognizable. The Subtropical Convergence (6) (the gyre center) is well situated and well defined.

The computed currents at the 80- to 100-m level, shown in figure 5(b), differ little from the surface currents, except in the equatorial region. At the lower level, the South Equatorial Current (1) is considerably weaker, whereas the Equatorial Countercurrent (7) is more pronounced. The development of a stronger subsurface equatorial countercurrent is interesting since such a phenomenon was not expected in a homogeneous model with

fairly coarse grid spacing and with a shallow, flat bottom. Furthermore, the model parameters tend to oppose development of subsurface countercurrents; the high vertical mixing coefficient $(0.01\ m^2/sec)$ and the low bottom drag coefficient (10^{-4}) tend to reduce vertical gradients in the velocity field, as can be seen in the rest of the region.

The vertically averaged currents in figure 5(c) show more clearly the computed circulation. The dominant features of the flow are three fairly well-defined gyres. The large anticyclonic gyre including the Gulf Stream, the North Equatorial Current, and the North Atlantic Current is bounded on the south by a smaller anticyclonic gyre, and on the north by a cyclonic gyre.

In table II, the approximate speeds of some of the computed currents are compared with data from reference 6. In general, the computed current speeds are somewhat lower than observed values. However, a homogeneous model cannot be expected to produce quantitatively accurate currents. The low current speeds in the Gulf Stream and the South Equatorial Current were attributed to land boundary treatment, grid resolution, and closed boundaries, as previously discussed.

CONCLUDING REMARKS

Calculations were performed for the near-surface currents of the North Atlantic Ocean on a finite-difference grid with 2.5° resolution in longitude and latitude and with five levels in the vertical direction. The model ocean was homogeneous with a uniform depth of 100 m and with a constrained upper surface. The model was driven by published mean wind stress data for the Northern Hemisphere summer. The northern (80° north) and southern (10° south) limits of the model were treated as closed boundaries.

The equations were integrated for approximately 40 simulation days, at which time the momentum equations over most of the ocean were essentially in steady state. The computed surface currents agreed for the most part with the observed currents, considering the simplicity of the study. Underprediction of current speeds was attributed to the lack of density stratification, to the smearing caused by the grid resolution, and to the model's treatment of flow along continental boundaries. The development of a strong subsurface countercurrent near the Equator was observed.

After about 40 simulation days, numerical difficulties at northern latitudes (above 60° north) led to instabilities in velocity. Minimal applied wind stress in the region of difficulty was probably the contributing factor to these numerical difficulties.

Langley Research Center
National Aeronautics and Space Administration
Hampton, Va. 23665
May 10, 1976

REFERENCES

1. Avis, Lee M.; Turner, Richard E.; and Rees, Thomas H.: A Generalized Tensor Formulation of Atmosphere and Seas Dynamics. NASA TR R-441, 1975.

2. Turner, Richard E.; Rees, Thomas H.; and Woodbury, Gerard E. (appendix A by Huw C. Davies): Adaptation of a General Circulation Model to Ocean Dynamics. NASA TN D-8258, 1976.

3. Cox, Michael D.: A Mathematical Model of the Indian Ocean. Deep-Sea Res. & Oceanogr. Abstr., vol. 17, no. 1, Feb. 1970, pp. 47-75.

4. Gross, M. Grant: Oceanography – A View of the Earth. Prentice-Hall, Inc., c.1972.

5. Hellerman, S.: An Updated Estimate of the Wind Stress on the World Ocean. Mon. Weather Rev., vol. 95, no. 9, Sept. 1967, pp. 607-626.

6. Oceanographic Atlas of the North Atlantic Ocean. Section I – Tides and Currents. Publ. No. 700, U.S. Naval Oceanogr. Off., 1965.

TABLE I.- MODEL PARAMETERS

Horizontal grid spacing, deg	2.5
Number of vertical levels	5
Depth (uniform), m	100
Layer thickness (uniform), m	20
Time step, sec	2600
Radius of Earth, r, km	6378
Angular velocity of Earth, ω, rad/sec	7.2919×10^{-5}
Vertical mixing coefficient, K_V, m^2/sec	0.01
Von Kármán constant for subgrid diffusion, K_o	0.4
Drag coefficient on bottom, C_D	0.0001
Temperature (uniform, constant), T, ^oC	0
Salinity (uniform, constant), S	35 $^o/_{oo}$
Initial velocity (uniform), U_α, m/sec	0
Wind stress (constant), τ_α	Summer mean

TABLE II.- COMPUTED AND OBSERVED CURRENT SPEEDS

Current	Current speed, m/sec	
	Computed, present study	Observed, reference 6
Gulf Stream	0.5 to 0.75	0.5 to 2.0
North Atlantic Current	0.2 to 0.4	0.25 to 0.5
North Equatorial Current	0.2 to 0.5	0.25 to 0.4
Equatorial Countercurrent	0.15 to 0.3	0.25 to 0.5
South Equatorial Current	0.2 to 0.55	0.25 to 1.5
Eastern North Atlantic Current	0.1 to 0.15	0.2 to 0.3

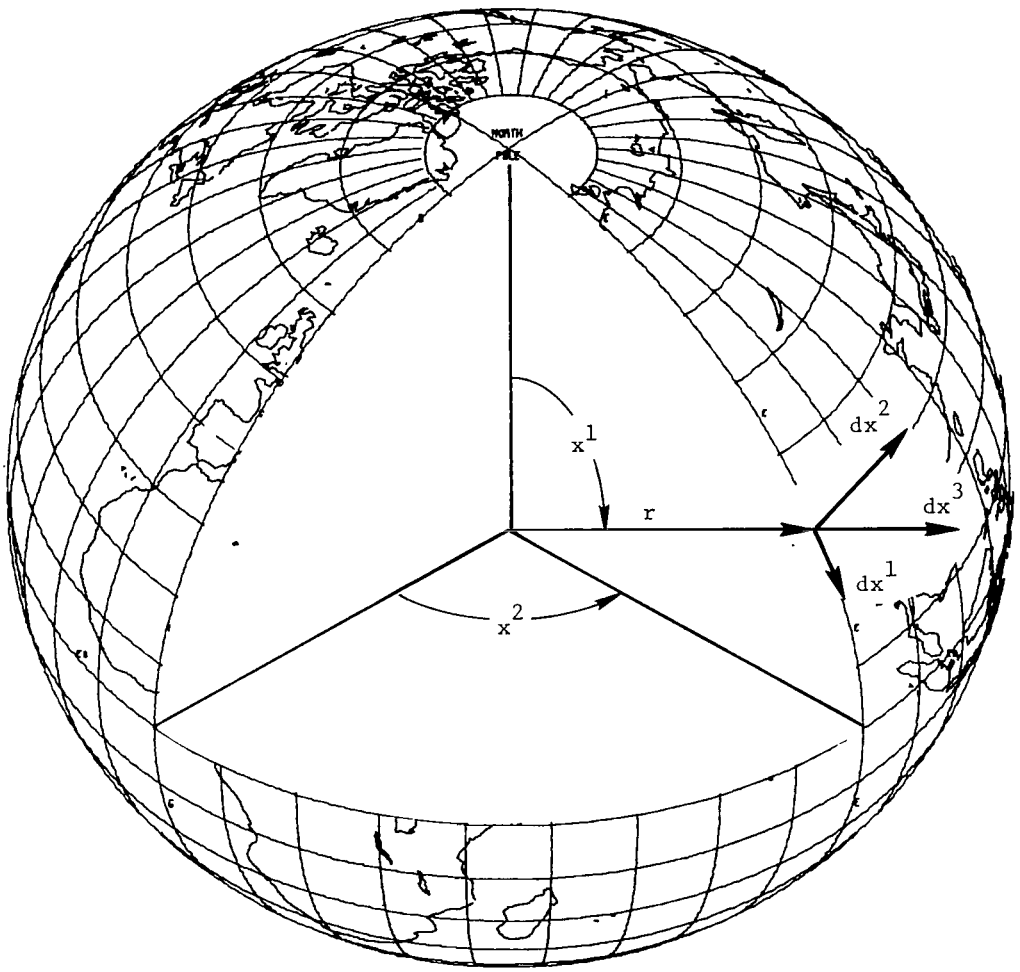

Figure 1.- Model coordinate system.

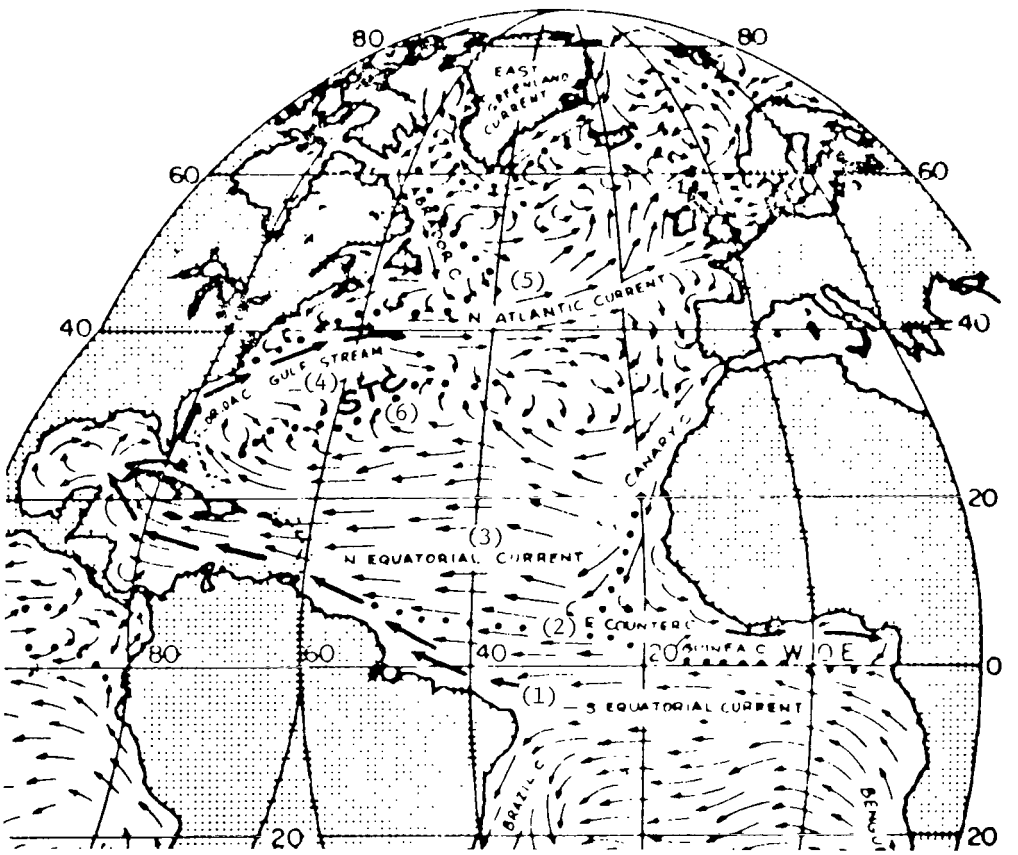

Figure 2.- Observed surface currents in the North Atlantic Ocean. (Reproduced from ref. 4 by permission of the publisher.)

Figure 3.- Model region and land boundary resolution. Hatched regions indicate artificially closed boundaries.

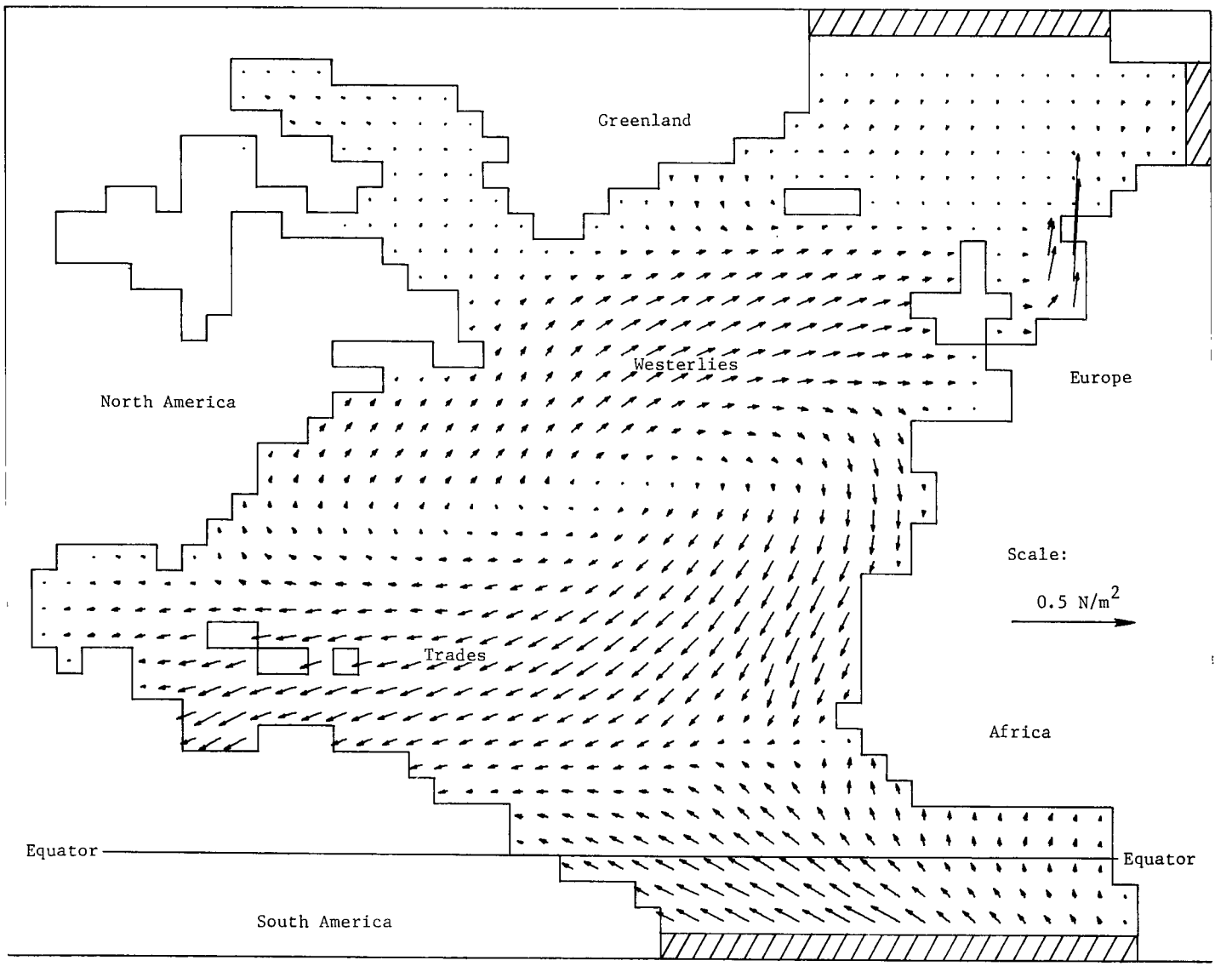

Figure 4.- Applied wind stress field; averages for Northern Hemisphere summer, interpolated from data given in reference 5. Hatched regions indicate artificially closed boundaries.

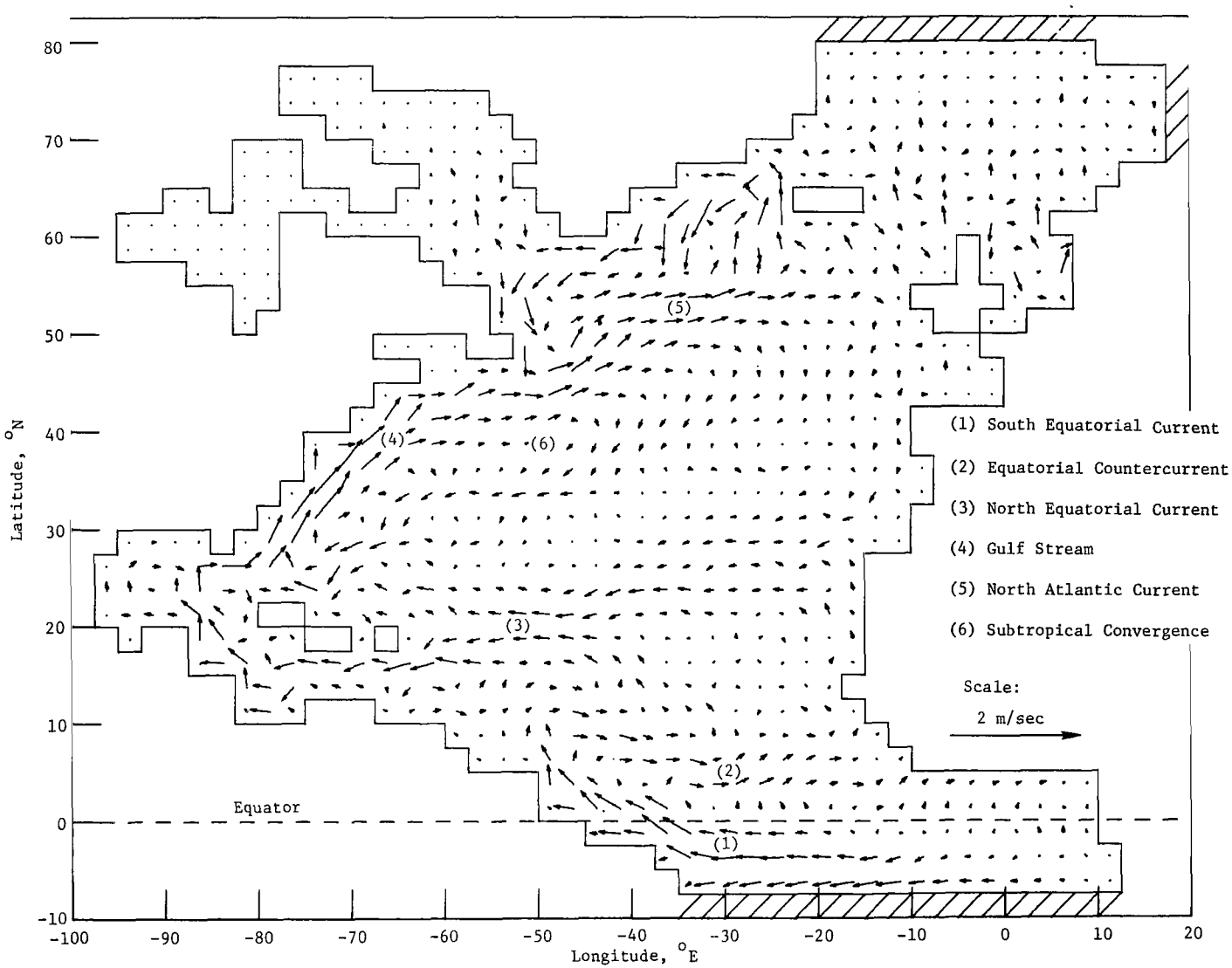

(a) In surface layer (0 to 20 m).

Figure 5.- Computed currents after approximately 40 simulation days. Hatched regions indicate artificially closed boundaries.

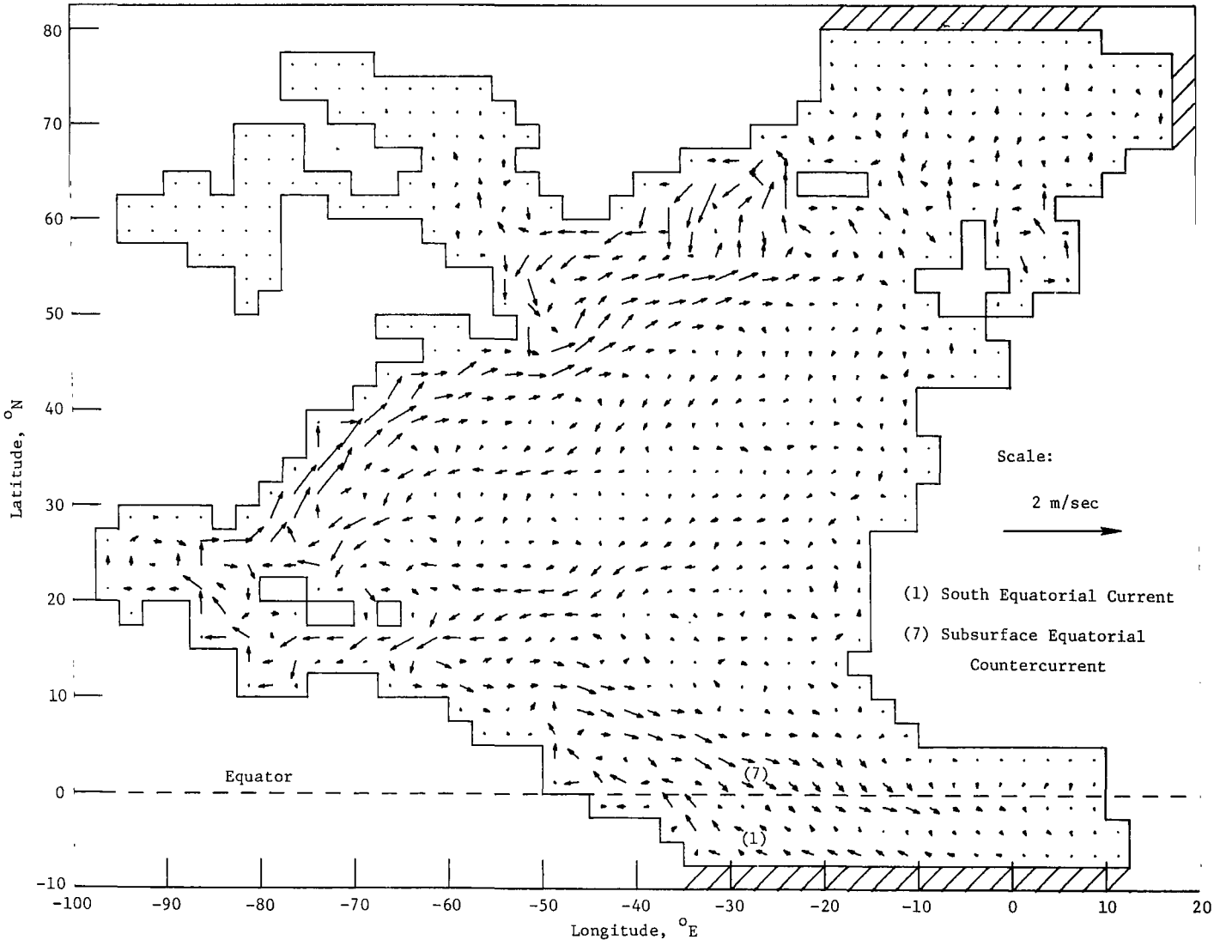

(b) In bottom layer (80 to 100 m).

Figure 5.- Continued.

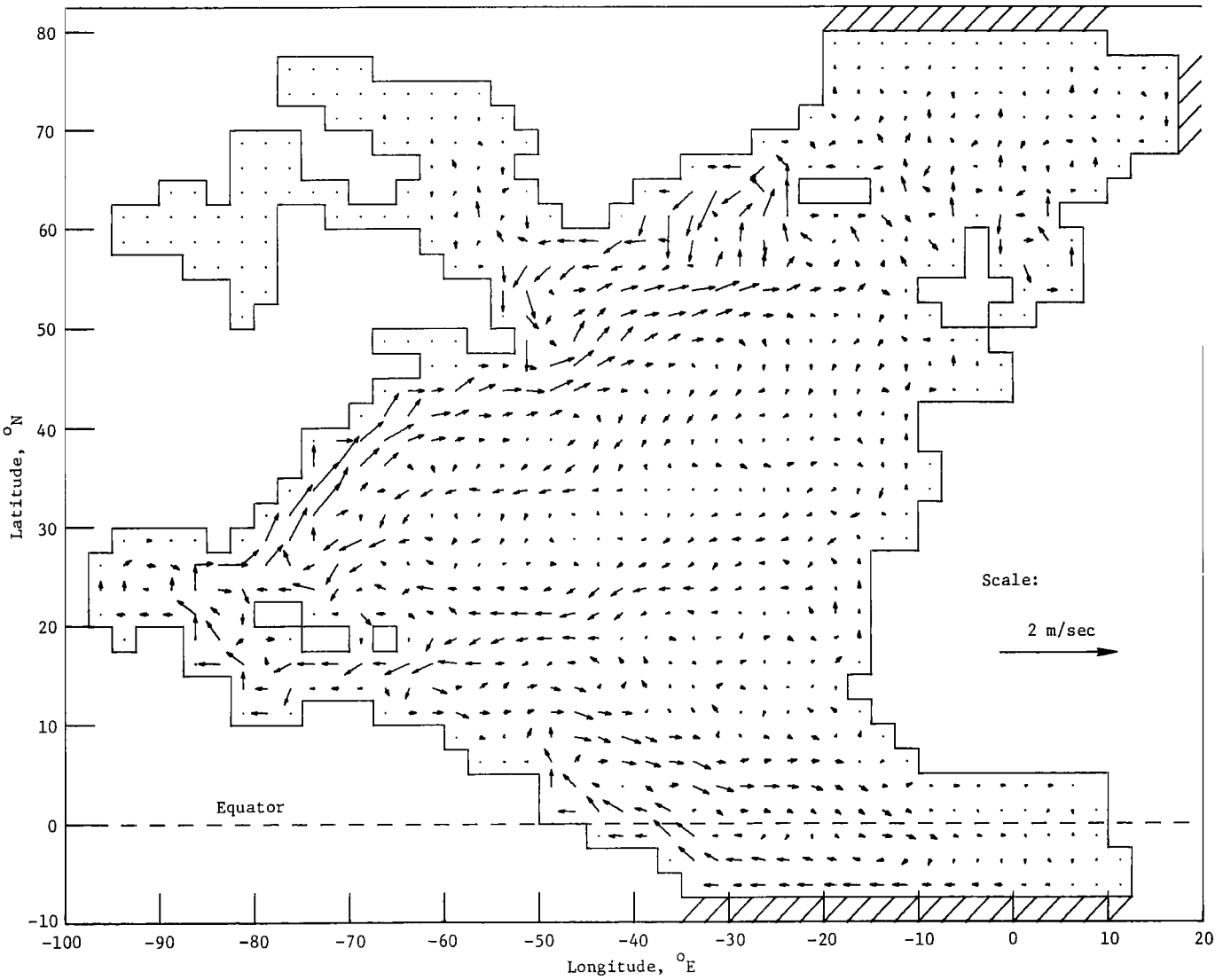

(c) Vertically averaged.

Figure 5.- Concluded.

"The aeronautical and space activities of the United States shall be conducted so as to contribute . . . to the expansion of human knowledge of phenomena in the atmosphere and space. The Administration shall provide for the widest practicable and appropriate dissemination of information concerning its activities and the results thereof."

—NATIONAL AERONAUTICS AND SPACE ACT OF 1958

NASA SCIENTIFIC AND TECHNICAL PUBLICATIONS

TECHNICAL REPORTS: Scientific and technical information considered important, complete, and a lasting contribution to existing knowledge.

TECHNICAL NOTES: Information less broad in scope but nevertheless of importance as a contribution to existing knowledge.

TECHNICAL MEMORANDUMS: Information receiving limited distribution because of preliminary data, security classification, or other reasons. Also includes conference proceedings with either limited or unlimited distribution.

CONTRACTOR REPORTS: Scientific and technical information generated under a NASA contract or grant and considered an important contribution to existing knowledge.

TECHNICAL TRANSLATIONS: Information published in a foreign language considered to merit NASA distribution in English.

SPECIAL PUBLICATIONS: Information derived from or of value to NASA activities. Publications include final reports of major projects, monographs, data compilations, handbooks, sourcebooks, and special bibliographies.

TECHNOLOGY UTILIZATION PUBLICATIONS: Information on technology used by NASA that may be of particular interest in commercial and other non-aerospace applications. Publications include Tech Briefs, Technology Utilization Reports and Technology Surveys.

Details on the availability of these publications may be obtained from:

SCIENTIFIC AND TECHNICAL INFORMATION OFFICE

NATIONAL AERONAUTICS AND SPACE ADMINISTRATION

Washington, D.C. 20546